Optimized Chiral Nucleon-Nucleon Interaction at Next-to-Next-to-Leading Order

A. Ekström,[1,2] G. Baardsen,[1] C. Forssén,[3] G. Hagen,[4,5] M. Hjorth-Jensen,[1,2,6] G. R. Jansen,[4,5] R. Machleidt,[7]
W. Nazarewicz,[5,4,8] T. Papenbrock,[5,4] J. Sarich,[9] and S. M. Wild[9]

[1]*Department of Physics and Center of Mathematics for Applications, University of Oslo, N-0316 Oslo, Norway*
[2]*National Superconducting Cyclotron Laboratory, Michigan State University, East Lansing, Michigan 48824, USA*
[3]*Department of Fundamental Physics, Chalmers University of Technology, SE-412 96 Göteborg, Sweden*
[4]*Physics Division, Oak Ridge National Laboratory, Oak Ridge, Tennessee 37831, USA*
[5]*Department of Physics and Astronomy, University of Tennessee, Knoxville, Tennessee 37996, USA*
[6]*Department of Physics and Astronomy, Michigan State University, East Lansing, Michigan 48824, USA*
[7]*Department of Physics, University of Idaho, Moscow, Idaho 83844, USA*
[8]*Faculty of Physics, University of Warsaw, ul. Hoża 69, 00-681 Warsaw, Poland*
[9]*Mathematics and Computer Science Division, Argonne National Laboratory, Argonne, Illinois 60439, USA*
(Received 19 March 2013; published 7 May 2013)

We optimize the nucleon-nucleon interaction from chiral effective field theory at next-to-next-to-leading order (NNLO). The resulting new chiral force $NNLO_{opt}$ yields $\chi^2 \approx 1$ per degree of freedom for laboratory energies below approximately 125 MeV. In the $A = 3, 4$ nucleon systems, the contributions of three-nucleon forces are smaller than for previous parametrizations of chiral interactions. We use $NNLO_{opt}$ to study properties of key nuclei and neutron matter, and we demonstrate that many aspects of nuclear structure can be understood in terms of this nucleon-nucleon interaction, without explicitly invoking three-nucleon forces.

Introduction.—Interactions from chiral effective field theory (EFT) employ symmetries and the pattern of spontaneous symmetry breaking of quantum chromodynamics [1,2]. In this approach, the exchange of pions within chiral perturbation theory yields the long-ranged contributions of the nuclear interaction, while short-ranged components are included as contact terms. The interaction is parametrized in terms of low-energy constants (LECs) that are determined by their fit to experimental data. The interactions from chiral EFT exhibit a power counting in the ratio Q/Λ, with Q being the low-momentum scale being probed and Λ the cutoff, which is of the order of 1 GeV. At next-to-next-to-leading order (NNLO), three-nucleon forces (3NFs) enter, while four-nucleon forces (4NFs) enter at next-to-next-to-next-to-leading order (N3LO). For laboratory energies below 125 MeV, the nucleon-nucleon (NN) force exhibits a quality of fit with $\chi^2 \approx 10/$datum at NNLO [3], while a high-precision potential N^3LO_{EM}, with a $\chi^2 \approx 1/$datum up to 290 MeV, was obtained by Entem and Machleidt [4].

The 3NFs at NNLO that accompany the current N3LO NN potentials play a pivotal role in nuclear structure calculations [5]. They determine the ground-state spin of ^{10}B [6], correctly set the drip line in oxygen isotopes [7,8], and make ^{48}Ca a doubly magic nucleus [9,10]. While it might seem surprising that smaller corrections at NNLO are so decisive for basic nuclear structure properties, the 3NF contains spin-orbit and tensor contributions that clearly are important for the currently employed chiral interactions. The contributions of 3NFs at N3LO have

also been worked out [11,12], and there are on-going efforts to compute even higher orders [13].

While the quest for higher orders is important, this approach will result in higher accuracy only if the optimization at lower orders was carried out accurately. Thus, it is important and timely to revisit the optimization question. We note in particular that the fits of the currently employed chiral interactions [3,4,14] date back about a decade and that there has been a considerable recent progress in developing tools for the derivative-free nonlinear least-squares optimization [15]. Furthermore, the quantification of theoretical uncertainties is a long-term objective of nuclear structure theory, and this requires a covariance analysis of the interaction parameters with respect to the experimental uncertainties of the nucleon-nucleon elastic scattering observables; see, for example, Refs. [15,16]. This Letter takes the first step toward this goal. We present a state-of-the-art optimization of the NN chiral EFT interaction at NNLO. This yields a much-improved χ^2 and a high-precision NN potential $NNLO_{opt}$. The 3NF at NNLO is adjusted to the binding energies in $A = 3, 4$ nuclei. We present computations of three-nucleon and four-nucleon bound states, and we employ $NNLO_{opt}$ to ground states and excited states in ^{10}B, masses and excited states of oxygen and calcium isotopes, and neutron matter.

Optimizing the NN interaction at NNLO.—For the optimization of the chiral NN interaction we use the Practical Optimization Using No Derivatives (for Squares) algorithm, POUNDERS [15], as implemented in [17]. This derivative-free algorithm employs a quadratic model and

TABLE I. Parameters of NNLO$_{opt}$ at $\Lambda = 500$ MeV and $\Lambda_{SFR} = 700$ MeV [3,21]: c_i (in GeV^{-1}), $\tilde{C}$ (in 10^4 GeV^{-2}), and C (in 10^4 GeV^{-4}). The number of decimal digits in the parameters ensure that the phase shifts, in degrees, are computed with a four decimal digit precision.

LEC	Value	LEC	Value	LEC	Value
c_1	$-0.918\,639\,53$	c_3	$-3.888\,687\,49$	c_4	$4.310\,327\,16$
$\tilde{C}^{pp}_{^1S_0}$	$-0.151\,366\,04$	$\tilde{C}^{np}_{^1S_0}$	$-0.152\,141\,09$	$\tilde{C}^{nn}_{^1S_0}$	$-0.151\,764\,75$
$C_{^1S_0}$	$2.404\,021\,94$	$C_{^3S_1}$	$0.928\,384\,66$	$\tilde{C}_{^3S_1}$	$-0.158\,434\,18$
$C_{^1P_1}$	$0.417\,045\,54$	$C_{^3P_0}$	$1.263\,390\,76$	$C_{^3P_1}$	$-0.782\,658\,50$
$C_{^3S_1-^3D_1}$	$0.618\,141\,42$	$C_{^3P_2}$	$-0.677\,808\,51$		

is particularly useful for computationally expensive objective functions. We optimize the three pion-nucleon (πN) couplings (c_1, c_3, c_4), and 11 partial wave contact parameters C and $\tilde{C}$, while we keep the axial-vector coupling constant g_A, the pion-decay constant f_π, and all masses fixed. In the optimization, we minimize the objective function

$$f(\vec{x}) = \sum_{q=1}^{N_q} \left(\frac{\delta_q^{NNLO}(\vec{x}) - \delta_q^{Nijm93}}{w_q} \right)^2, \qquad (1)$$

where δ^{NNLO} are NNLO phase shifts, δ^{Nijm93} are experimental phase shifts from the Nijmegen multienergy partial-wave analysis [18], $\vec{x}$ denotes the parameters of the chiral interaction, and w_q are weighting factors. Note that Eq. (1) is not the χ^2 with respect to experimental data. The actual χ^2 is calculated following the POUNDERS optimization. The phase shifts δ^{NNLO} are computed from R-matrix inversion, and in the proton-proton (pp) channels we include the Coulomb interaction [19,20]. The contact terms are optimized to reproduce the Nijmegen phase shifts for each corresponding partial wave, while keeping the c_i's fixed. For the contacts, the weight w_q scales with the third power of the relative momentum q, while for the c_i's, we employ the uncertainties quoted in the Nijmegen analysis [18]. This approach can be justified by a physical argument: for the peripheral waves the higher energies still represent longer-range physics, and the need for a pedantic agreement with lower energy phase shifts can be weakened. The πN couplings c_1, c_3, and c_4 were simultaneously optimized to the peripheral partial waves $^1D_2$, $^3D_2$, $^3F_2$, E_2, $^3F_3$, $^1G_4$, and $^3F_4$. Note that the NNLO contact terms do not contribute to orbital angular momenta $L \geq 2$. We do not include other peripheral waves from the Nijmegen study since they carry extremely small uncertainties, which lead to a very noisy objective function.

Table I summarizes the optimization results. Our values should be compared with the πN couplings as determined from πN scattering data, where $c_1 = -0.81 \pm 0.15$, $c_3 = -4.69 \pm 1.34$, and $c_4 = +3.40 \pm 0.04$ have been obtained [22]. Thus, POUNDERS yields values for c_1 and c_3 that agree well with the empirical determination from πN scattering. The c_4 value, however, deviates significantly from its empirical value. The same trend was found in the construction of the N^{3}LO [4] NN interaction. A detailed statistical

sensitivity analysis of the LECs with uncertainty quantification will be presented in Ref. [23].

Table II shows the χ^2/datum for NNLO$_{opt}$ at various laboratory energy bins. The quality of the fit is particularly good for energies below 125 MeV. For comparison, the np NNLO interaction of Ref. [3] yields χ^2/datum of 12–27 in the range $\Lambda = 600/700 - 450/500$ MeV at energies up to 290 MeV.

Around energies of 144 MeV there exist two data sets of pp differential cross sections with a very high precision (0.5% error) [25] (47 data points). The total number of pp data in the energy interval 125–183 MeV is 343. The unusual precision of those 47 data points distorts the χ^2/datum for this interval. For this reason, Table II also shows the results without the high-precision data.

Two comments are in order. First, the χ^2 with respect to scattering observables is lower when the $^1P_1$ phase shifts are weighted with the uncertainties from the Nijmegen analysis. The P waves are accurately reproduced only when going to N^{3}LO [4]. Second, the $^3S_1 - ^3D_1$ coupled channel is optimized with the additional constraint of reproducing the deuteron binding energy. The remaining deuteron observables, as well as the $^1S_0$ scattering observables, are predictions and reproduce the experimental values well; see Table III.

Figure 1 shows some np phase shifts of NNLO$_{opt}$ and compares them with phase shifts from other potentials and partial wave analyses. Apart from the ^3P waves, the phase shifts of NNLO$_{opt}$ closely agree with those obtained at N^{3}LO. Note, however, that these deviations do not spoil the good χ^2 at laboratory energies below 125 MeV.

Three-nucleon forces also appear at NNLO, and two additional LECs (c_D and c_E) enter. These are determined from calculations in the three-nucleon and four-nucleon

TABLE II. χ^2/datum for NNLO$_{opt}$ at $\Lambda = 500$ MeV and $\Lambda_{SFR} = 700$ MeV [3,21] with respect to the np and pp 1999 databases [24]. The values without the high-precision data sets [25] are marked by asterisks.

T_{lab} (MeV)	0–35	35–125	125–183	183–290	0–290
pp χ^2/datum	1.11	1.56	$\begin{cases}23.95\\4.35^*\end{cases}$	29.26	$\begin{cases}17.10\\14.03^*\end{cases}$
np χ^2/datum	0.85	1.17	1.87	6.09	2.95

TABLE III. Scattering lengths a and effective ranges r (both in fm). The superscripts N and C for the proton-proton observables refer to nuclear forces and Coulomb-plus-nuclear forces, respectively. B_D, r_D, Q_D, and P_D denote the deuteron binding energy, radius, quadrupole moment, and D-state probability, respectively. Q_D and r_D are calculated without meson-exchange currents and relativistic corrections.

	N^3LO_{EM}	$NNLO_{opt}$	Exp.	Ref.
a_{pp}^C	−7.8188	−7.8174	−7.8196(26)	[26]
			−7.8149(29)	[27]
r_{pp}^C	2.795	2.755	2.790(14)	[26]
			2.769(14)	[27]
a_{pp}^N	−17.083	−17.825		
r_{pp}^N	2.876	2.817		
a_{nn}	−18.900	−18.889	−18.95(40)	[28,29]
r_{nn}	2.838	2.797	2.75(11)	[30]
a_{np}	−23.732	−23.749	−23.740(20)	[24]
r_{np}	2.725	2.684	2.77(5)	[24]
B_D (MeV)	2.224 575	2.224 582	2.224 575(9)	[24]
r_D (fm)	1.975	1.967	1.975 35(85)	[31]
Q_D (fm^2)	0.275	0.272	0.2859(3)	[24]
P_D (%)	4.51	4.05		

systems. We find that the binding energies of ^{3}H, ^{3}He, and ^{4}He do not uniquely determine c_D and c_E, and the parametric dependence of both LECs is very similar to those found in previous studies [6,32,33]. Therefore, we choose $c_D = -0.2$ guided by the triton half life [33] and obtain $c_E = -0.36$ from optimization to the binding energies. The resulting point charge radii of ^{4}He are also in good agreement with experiment; see Table IV.
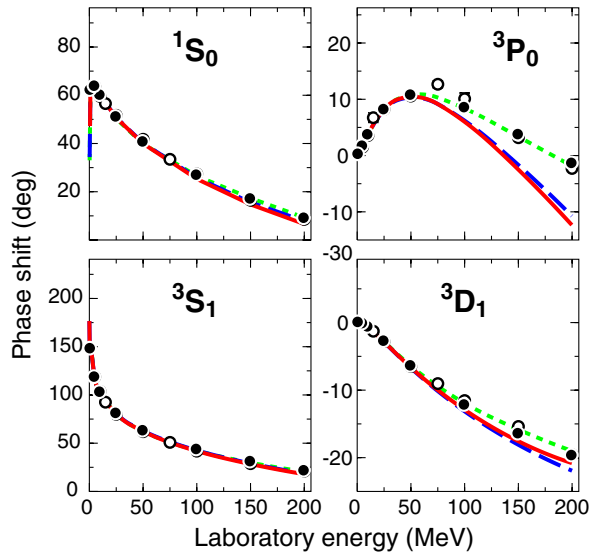

FIG. 1 (color online). Computed np phase shifts of the optimized NNLO potential of this work (solid, red line), the NNLO potential of Ref. [3] (dashed, blue line), and the N^{3}LO potential [4] (green, dotted line) compared with the Nijmegen phase shift analysis [18] (solid dots) and the VPI/GWU analysis SM99 [43] (open circles).

TABLE IV. Ground-state energies (in MeV) and point proton radii (in fm) for ^{3}H, ^{3}He, and ^{4}He using the NNLO$_{opt}$ with and without the NNLO 3NF interaction for $c_D = -0.20$ and $c_E = -0.36$.

	$E(^3H)$	$E(^3He)$	$E(^4He)$	$r_p(^4He)$
NNLO	−8.249	−7.501	−27.759	1.43(8)
NNLO+NNN	−8.469	−7.722	−28.417	1.43(8)
Experiment	−8.482	−7.717	−28.296	1.467(13)

Performance of NNLO$_{opt}$ *for light- and medium-mass nuclei and neutron matter.*—In this Letter, we apply NNLO$_{opt}$ to ^{10}B, isotopes of oxygen and calcium, and neutron matter. The considered systems are particularly interesting because the current NN chiral interactions at N^{3}LO completely fail to describe key aspects of their structure.

To study the ground state and first excited state in ^{10}B, we carry out no-core shell model (configuration interaction) calculations [34] using the bare NNLO$_{opt}$ in model spaces of up to $N_{max} = 10$ harmonic oscillator (HO) shells ($10\,\hbar\Omega$) above the unperturbed configuration. These model spaces are not large enough to provide fully converged results for the ground state and first excited state of ^{10}B. Still, the variational upper bounds for the energies are −54.35 MeV for the 1^+ state and −54.32 MeV for the 3^+ state. The energies are very close, in contrast to N^{3}LO$_{EM}$, which yields a level spacing of about 1.2 MeV between the $J^\pi = 1^+$ ground state and the $J^\pi = 3^+$ excited state [6].

Chiral NN interactions at N^{3}LO fail to explain the neutron drip-line in oxygen isotopes, and 3NFs have been the key element for understanding the structure of nuclei around ^{24}O [7,8]. Figure 2 shows the experimental ground-state energies of oxygen isotopes and compares the results from coupled-cluster (CC) computations in the Λ triples approximation [35–37]. Our CC calculations employ a Hartree-Fock basis built from $N_{max} = 15$ HO shells at $\hbar\Omega = 20$ MeV. Because of the "softness" of NNLO$_{opt}$, this model space is sufficiently large to converge the ground states and excited states of the nuclei
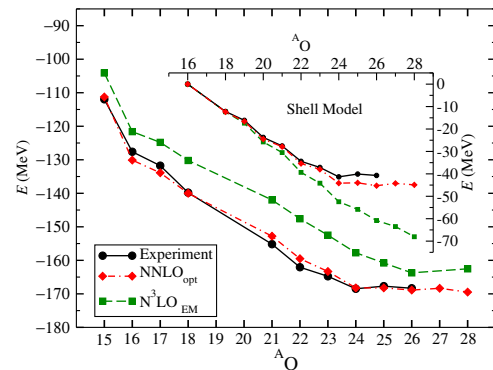

FIG. 2 (color online). The ground-state energies of oxygen isotopes obtained in CC with the NNLO$_{opt}$ and N^{3}LO$_{EM}$ interactions compared with experiment. The inset shows SM results.
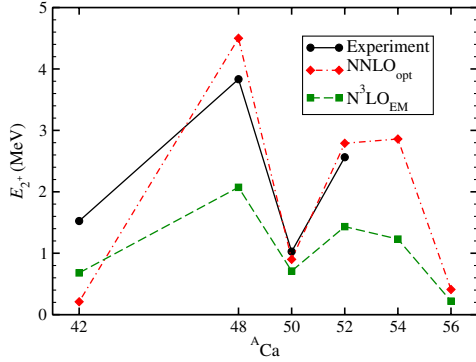
FIG. 3 (color online). The first 2_1^+ state in selected calcium isotopes obtained in CC with the NNLO$_{opt}$ and N^{3}LO$_{EM}$ interactions compared with experiment.

considered. In addition, we performed shell-model (SM) calculations assuming the closed ^{16}O core with an effective interaction derived from many-body perturbation theory to third order in the interaction and including folded diagrams [38]. For the SM calculations, the single-particle energies were taken from the experimental ^{17}O spectrum. In both CC and SM, NNLO$_{opt}$ results are close to experiment. In contrast, the N^{3}LO$_{EM}$ case requires 3NFs to provide reasonable description of measured values.

Now we consider the heavy isotopes of calcium. Here, ^{48}Ca is doubly magic, ^{52}Ca exhibits a soft subshell closure, and ^{54}Ca is predicted to have an even softer subshell closure [10]. A signature of shell closure is the location of the first 2^+ state. We employed CC equation-of-motion methods within the singles and doubles approximation [37,39] to compute the first 2^+ state in the calcium isotopes. Figure 3 shows that N^{3}LO$_{EM}$ fails to describe the location of the first 2^+ state in ^{40,48,50,52,54,56}Ca. In contrast, NNLO$_{opt}$ yields ^{48}Ca as a doubly magic nucleus and predicts subshell closures in ^{52,54}Ca. The NNLO$_{opt}$ overbinds the calcium isotopes by about 1 MeV per nucleon. In particular, ^{40,48,52}Ca are overbound by 1.03, 1.06, and 1.04 MeV per nucleon, respectively. That is, the excess energy per nucleon is fairly constant; hence, NNLO$_{opt}$ reproduces binding energy differences, such as neutron-separation energies and low-lying excited states, rather well.

The complete description of nuclei at NNLO also requires 3NFs. We computed the first 2^+ state in ^{22,24}O and in ^{48}Ca with the 3NF compatible with the NNLO$_{opt}$ interaction. The matrix elements of the 3NF are expensive computationally, and we must at present limit their calculation to three-body energies up to $e_{3\,max} = 2n_a + l_a + 2n_b + l_b + 2n_c + l_c = 14$. (Recall that we employ 15 major harmonic oscillator shells for the NN interaction.) We also used the normal ordered two-body approximation for the 3NF [40,41] with respect to a Hartree-Fock reference. With the restriction of $e_{3\,max} = 14$, we were not able to obtain fully converged results for the binding energies of oxygen and calcium isotopes. However, excitation energies relative to the ground state converge somewhat better.
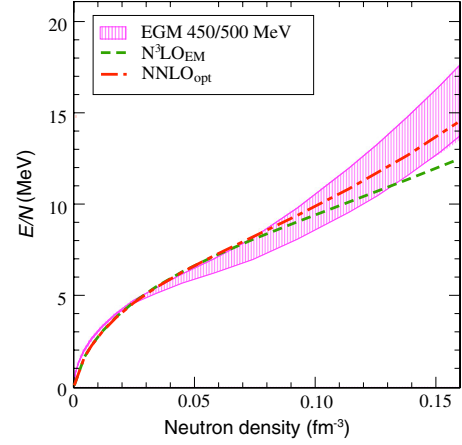

FIG. 4 (color online). Energy per nucleon for neutron matter for NNLO$_{opt}$ and N^{3}LO$_{EM}$ [4]. The calculations used the CC method with the inclusion of particle-particle ladders and a continuous single-particle spectrum. The shaded area (EGM) shows uncertainty bands for the N^{3}LO chiral effective field theory calculations of Ref. [42], including 3NFs.

Our results for the first 2^+ state in ^{22,24}O and in ^{48}Ca are 2.3(3), 3.5(5), and 4.8(7) MeV, respectively. We estimate the uncertainty by varying $\hbar\Omega$ in the interval 16–22 MeV. The results obtained by using NNLO$_{opt}$ NN interaction alone yields 2.5, 5.0, and 4.5 MeV in ^{22,24}O and ^{48}Ca, respectively. These preliminary results suggest that the 3NFs may not dramatically change the results that were obtained with the NNLO$_{opt}$ NN interaction alone.

It is instructive to compare the predictions of NNLO$_{opt}$ and N^{3}LO$_{EM}$ for the neutron matter equation of state at subsaturation densities with the results of *ab initio* calculations of Refs. [42]. Figure 4 shows that the performance of NNLO$_{opt}$ is on par with the EGM results of Ref. [42], which take into account the effects of 3NFs and 4NFs. The predictions of N^{3}LO$_{EM}$ deviate from other results at higher densities.

Conclusions.—We constructed the new NN chiral EFT interaction NNLO$_{opt}$ at next-to-next-to-leading order using the optimization tool POUNDERS in the phase-shift analysis. The optimization of the low-energy constants in the NN sector at NNLO yields a χ^2/datum of about one for laboratory scattering energies below 125 MeV. The NNLO$_{opt}$ NN interaction yields very good agreement with binding energies and radii for $A = 3$, 4 nuclei. Key aspects of nuclear structure, such as excitation spectra, the position of the neutron drip line in oxygen, shell-closures in calcium, and the neutron matter equation of state at subsaturation densities, are reproduced by NNLO$_{opt}$ interaction alone, without resorting to 3NFs. We performed the initial calculation of the first 2^+ states in ^{22,24}O and ^{48}Ca with NNLO$_{opt}$ supplemented by a 3NF and found the effects of 3NFs to be small and in good agreement with experimental excitation energies. The precise role of 3NFs in medium-mass nuclei, the quantification of theoretical uncertainties, and optimizations at higher-order chiral interactions will be addressed in forthcoming investigations.

[1] U. van Kolck, Phys. Rev. C **49**, 2932 (1994).
[2] E. Epelbaum, H.-W. Hammer, and U.-G. Meißner, Rev. Mod. Phys. **81**, 1773 (2009); R. Machleidt and D. Entem, Phys. Rep. **503**, 1 (2011).
[3] E. Epelbaum, W. Glöckle, and U.-G. Meißner, Eur. Phys. J. A **19**, 401 (2004); E. Epelbaum, A. Nogga, W. Glöckle, H. Kamada, U.-G. Meißner, and H. Witała, Eur. Phys. J. A **15**, 543 (2002).
[4] D. R. Entem and R. Machleidt, Phys. Rev. C **68**, 041001(R) (2003).
[5] H.-W. Hammer, A. Nogga, and A. Schwenk, Rev. Mod. Phys. **85**, 197 (2013).
[6] P. Navrátil, V. G. Gueorguiev, J. P. Vary, W. E. Ormand, and A. Nogga, Phys. Rev. Lett. **99**, 042501 (2007).
[7] T. Otsuka, T. Suzuki, J. D. Holt, A. Schwenk, and Y. Akaishi, Phys. Rev. Lett. **105**, 032501 (2010).
[8] G. Hagen, M. Hjorth-Jensen, G. R. Jansen, R. Machleidt, and T. Papenbrock, Phys. Rev. Lett. **108**, 242501 (2012).
[9] J. D. Holt, T. Otsuka, A. Schwenk, and T. Suzuki, J. Phys. G **39**, 085111 (2012).
[10] G. Hagen, M. Hjorth-Jensen, G. R. Jansen, R. Machleidt, and T. Papenbrock, Phys. Rev. Lett. **109**, 032502 (2012).
[11] S. Ishikawa and M. R. Robilotta, Phys. Rev. C **76**, 014006 (2007).
[12] V. Bernard, E. Epelbaum, H. Krebs, and U.-G. Meißner, Phys. Rev. C **77**, 064004 (2008); V. Bernard, E. Epelbaum, H. Krebs, and U.-G. Meißner, Phys. Rev. C **84**, 054001 (2011).
[13] H. Krebs, A. Gasparyan, and E. Epelbaum, Phys. Rev. C **85**, 054006 (2012).
[14] E. Epelbaum, A. Nogga, W. Glöckle, H. Kamada, U.-G. Meißner, and H. Witała, Phys. Rev. C **66**, 064001 (2002).
[15] M. Kortelainen, T. Lesinski, J. Moré, W. Nazarewicz, J. Sarich, N. Schunck, M. V. Stoitsov, and S. Wild, Phys. Rev. C **82**, 024313 (2010).
[16] P.-G. Reinhard and W. Nazarewicz, Phys. Rev. C **81**, 051303 (2010).
[17] T. Munson, J. Sarich, S. M. Wild, S. Benson, and L. C. McInnes, Technical Memorandum ANL/MCS-TM-322, Argonne National Laboratory, Argonne, Illinois (2012), see http://www.mcs.anl.gov/tao.
[18] V. G. J. Stoks, R. A. M. Klomp, M. C. M. Rentmeester, and J. J. de Swart, Phys. Rev. C **48**, 792 (1993).
[19] C. M. Vincent and S. C. Phatak, Phys. Rev. C **10**, 391 (1974).
[20] D. H. Lu, T. Mefford, R. H. Landau, and G. Song, Phys. Rev. C **50**, 3037 (1994).
[21] E. Epelbaum, Prog. Part. Nucl. Phys. **57**, 654 (2006).
[22] P. Büttiker and U.-G. Meißner, Nucl. Phys. **A668**, 97 (2000).
[23] A. Ekström et al. (to be published).
[24] R. Machleidt, Phys. Rev. C **63**, 024001 (2001).
[25] G. Cox, G. Eaton, C. V. Zyl, O. Jarvis, and B. Rose, Nucl. Phys. **B4**, 353 (1968), 21 pp diff. cross section data at 144.1 MeV.O. Jarvis, C. Whitehead, and M. Shah, Phys. Lett. **36B**, 409 (1971), 26 pp diff. cross section data at 144.0 MeV.
[26] J. R. Bergervoet, P. C. van Campen, W. A. van der Sanden, and J. J. de Swart, Phys. Rev. C **38**, 15 (1988).
[27] W. A. van der Sanden, A. H. Emmen, and J. J. de Swart, Tech. Rep., Nijmegen (1983), unpublished.
[28] D. E. Gonzalez Trotter et al., Phys. Rev. C **73**, 034001 (2006).
[29] Q. Chen et al., Phys. Rev. C **77**, 054002 (2008).
[30] G. Miller, B. Nefkens, and I. Šlaus, Phys. Rep. **194**, 1 (1990).
[31] A. Huber, T. Udem, B. Gross, J. Reichert, M. Kourogi, K. Pachucki, M. Weitz, and T. W. Hänsch, Phys. Rev. Lett. **80**, 468 (1998).
[32] A. Nogga, P. Navrátil, B. R. Barrett, and J. P. Vary, Phys. Rev. C **73**, 064002 (2006).
[33] D. Gazit, S. Quaglioni, and P. Navrátil, Phys. Rev. Lett. **103**, 102502 (2009).
[34] B. Barrett, P. Navrátil, and J. P. Vary, Prog. Part. Nucl. Phys. **69**, 131 (2013).
[35] S. A. Kucharski and R. J. Bartlett, J. Chem. Phys. **108**, 5243 (1998).
[36] A. G. Taube and R. J. Bartlett, J. Chem. Phys. **128**, 044110 (2008).
[37] G. Hagen, T. Papenbrock, D. J. Dean, and M. Hjorth-Jensen, Phys. Rev. C **82**, 034330 (2010).
[38] M. Hjorth-Jensen, T. T. S. Kuo, and E. Osnes, Phys. Rep. **261**, 125 (1995).
[39] G. R. Jansen, M. Hjorth-Jensen, G. Hagen, and T. Papenbrock, Phys. Rev. C **83**, 054306 (2011).
[40] G. Hagen, T. Papenbrock, D. J. Dean, A. Schwenk, A. Nogga, M. Włoch, and P. Piecuch, Phys. Rev. C **76**, 034302 (2007).
[41] S. Binder, J. Langhammer, A. Calci, P. Navrátil, and R. Roth, Phys. Rev. C **87**, 021303 (2013).
[42] I. Tews, T. Krüger, K. Hebeler, and A. Schwenk, Phys. Rev. Lett. **110**, 032504 (2013).
[43] R. A. Arndt, I. I. Strakovsky, and R. L. Workman (1999), SAID, Scattering Analysis Interactive Dial-in computer facility, George Washington University (formerly Virginia Polytechnic Institute), solution SM99 (Summer 1999); for more information see, e.g., R. A. Arndt, I. I. Strakovsky, and R. L. Workman, Phys. Rev. C **50**, 2731 (1994).